

Raman Spectroscopy Revealed Cell Passage-Dependent Distinct Biochemical Alterations in Radiation-Resistant Breast Cancer Cells

Sukanya Rauniyar, Kshama Pansare, Asmita Sharda, Saurav Raj Singh, Panchali Saha, Murali Krishna Chilakapati,* and Sanjay Gupta*



Cite This: *ACS Omega* 2023, 8, 5522–5532



Read Online

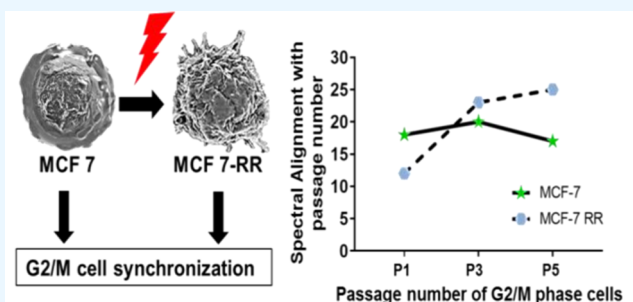
ACCESS |

Metrics & More

Article Recommendations

Supporting Information

ABSTRACT: Recapitulating radioresistant cell features in pertinent cell line models is essential for deciphering fundamental cellular mechanisms. The limited understanding of passage and cell cycle phases on radioresistant cells revived post-cryopreservation led us to investigate the effect of sub-culturing in parental and radioresistant MCF-7 cells. In this study, the radioresistant cells showed high-intensity nucleic acid and cytochrome bands, which are potentially a radiation-induced spectral marker. Raman spectroscopy data showed dynamic biochemical alterations in revived radioresistant G₂/M synchronized cells at early cell passages 1 and 3 with stabilization at a latter cell passage, 5. The study highlights the importance of cell passaging and cell cycle phases in potentially changing the biochemical parameters during in vitro experiments after the revival of radioresistant cells post-cryopreservation.



Raman spectra stabilizes at later passage in G₂/M phase MCF7-RR cells

INTRODUCTION

Radiotherapy as a standalone treatment or in combination with surgery, chemotherapy, or hormone therapy is recommended for breast cancer patients, in neo-adjuvant and adjuvant settings.¹ Although a well-defined treatment plan is tailored for an individual patient, the outcome of radiotherapy is often hindered by resistance to radiation, leading to recurrence. Cell line representatives of molecular subtypes of breast cancer such as estrogen receptor (ER+/-), progesterone receptor (PR +/-), and Herceptin 2 amplification (Her2+/-) have inherently different radio sensitivities; nevertheless, in vitro models are developed for acquired radioresistance for studying the molecular mechanism that contributes to resistance.²

Several in vitro studies are ongoing to understand the mechanisms underlying acquired radioresistance and develop newer strategies to circumvent clinical problems.^{1b,2d,3} These established radioresistant cell lines are cryopreserved for long-term storage and revived as and when needed. However, these freeze–thaw cycles induce different kinds of stress on the reviving cells, such as osmosis by the cryoprotectant, cold shock by alterations in temperature, and oxidative stress due to reactive oxygen species, which eventually damage the cells.⁴ Most of these processes lead to increased cell death due to apoptosis (as opposed to necrosis). Previous studies have shown that multiple factors are implicated in the development of radioresistance, like deregulated signaling pathways (e.g., PI3K/AKT, NF-κB) and alterations in cancer metabolism.⁵ Thus, exposure to extra- or intracellular stress post-cryopreservation and revival will disrupt

cellular homeostasis and cause the engagement of signaling pathways that serve to rebalance biochemical processes within the cell. As is known, these changes are dynamic and might alter with time. Considering that the reviving cells are under stress in the early passages, determining the appropriate passage number for performing experiments is crucial for obtaining reliable and reproducible results. Earlier studies have shown that the Raman spectrometer, a vibrational spectroscopic tool, has shown immense potential in cancer diagnosis, surgical margin assessment, recurrence prediction, and quality assessment of tumor biospecimens and to assess fractionated radiation dose response in ex vivo tissues and in vitro cells.⁶ The parental cell line characteristics, such as morphology, growth rate, tumorigenicity, gene and protein expression patterns, and cellular signaling pathways, alter with increasing cell passage numbers.⁷ Even after establishing the acquired radioresistance in cell lines, performing experiments at appropriate cell passages is often overlooked during in vitro studies.

Therefore, understanding the response to radiation with differing cell passage and the importance of cell cycle phases would provide crucial information about the biochemical

Received: October 21, 2022

Accepted: January 26, 2023

Published: February 3, 2023



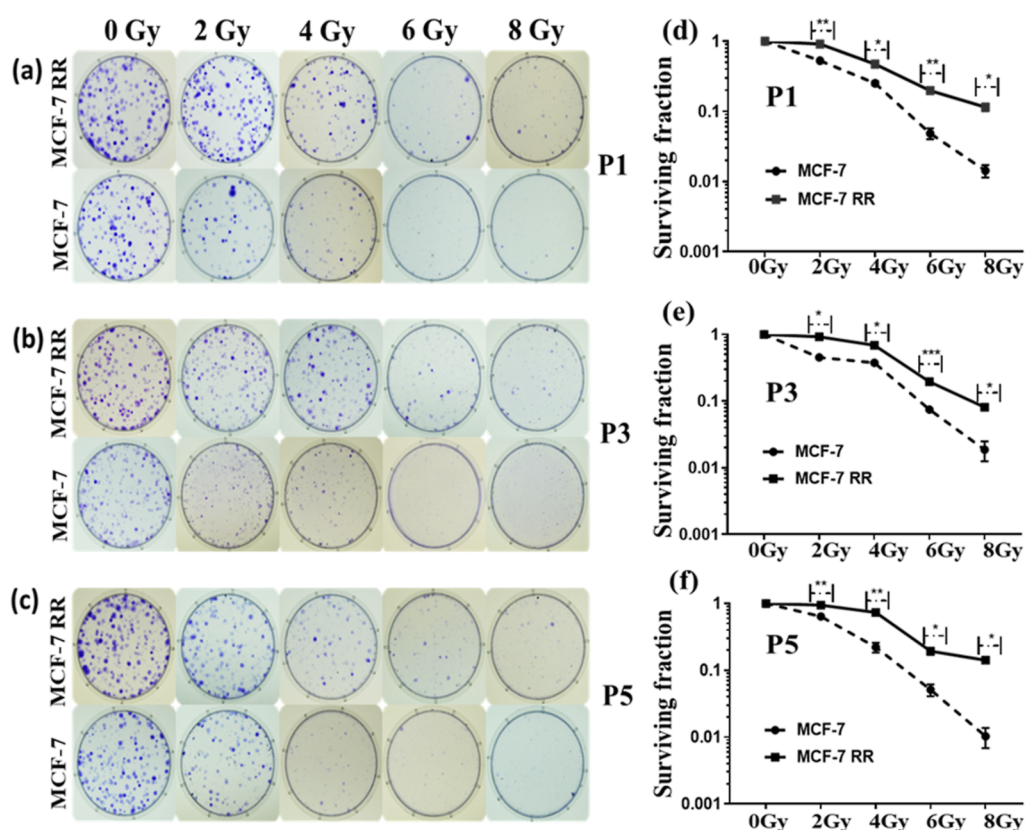


Figure 1. Development and characterization of the MCF7-RR cell line. (a–c) Representative images for Clonogenic assay performed in parental MCF7 and MCF7-RR cell lines at passages 1, 3, and 5. Cells were irradiated with a single fraction of 2, 4, 6, and 8 Gy radiation doses. The number of colonies was counted and data were analyzed. (d–f) Graph depicting enhanced surviving fraction of MCF7 and MCF7-RR cell lines at passage 1 (P1), passage 3 (P3), and passage 5 (P5) after irradiation with a single fraction of 2, 4, 6, and 8 Gy radiation dose. Student's t-test was used for statistical analysis, * $P < 0.05$, ** $P < 0.01$, *** $P < 0.001$. $n = 3$ for all experiments. Error bars represent the mean \pm SD of three experiments.

changes in cells. In this study, we report an analysis of the morphological and biochemical alterations that occur in acquired radioresistant cells as they are cultured in vitro through different passages post-cryopreservation. These analyses are performed on different cell cycle phases of cells and varying passage numbers that occur upon the maintenance of acquired radioresistant cells. Unique Raman spectral features were observed in radioresistant MCF-7 cells compared to the parental MCF-7 cells. Further, multivariate analysis shows distinct stratification of the highly radiosensitive G_2/M and moderately sensitive G_0/G_1 phases across different cell passages. Our findings demonstrate that the earlier cell passages 1 and 3 show dynamic biochemical alterations on cell revival, whereas in cell passage 5, these alterations stabilize. Based on the findings, we propose performing in vitro studies on revived radioresistant cell lines at a later passage to understand varying radiation-associated changes better.

MATERIALS AND METHODS

Cell Lines and Reagents. MCF-7 and MCF7-RR cell lines were cultured in DMEM media (Invitrogen) supplemented with an antimycotic antibiotic solution (Himedia), 10% fetal bovine serum (FBS; Gibco), and 2 mM glutamine (Sigma). Cell lines were maintained at 37 °C and in a 5% CO_2 atmosphere.

Development of Radioresistant Cell Line and Cell Synchronization. The radioresistant MCF-7 cell line (MCF7-RR) was prepared by giving fractionated irradiation with a cumulative dose of 20 Gy in 10 fractions of 2 Gy each. A Co-60

radioactive source machine Bhabhatron-II (Panacea Medical Technologies Ltd. and Bhabha Atomic Research Centre, Mumbai, India) installed at the Department of Radiation Oncology was used to deliver radiation to the cells. Cells were synchronized in the G_0/G_1 phase by serum starvation using 0.02% serum for 72 h, followed by 6 h of serum release in the mitotic phase and incubation with 200 ng/mL nocodazole for 18 h.

Clonogenic Assay. Cells (~500) were seeded in a 6-well plate, irradiated at 0, 2, 4, 6, and 8 Gy, and cultured for 14 days at 37 °C and 5% CO_2 . Colonies were washed with phosphate-buffered saline and fixed in 4% paraformaldehyde (Sigma) for 20 min. The colonies were stained using 0.5% crystal violet, and clones containing >50 cells were considered for analysis. The plating efficiency was calculated as described,⁷ and the surviving fraction was calculated for MCF-7 and MCF7-RR cell lines.

Cellular Morphology and Immunofluorescence Microscopy. Morphological analysis was done using phase-contrast microscopy (Zeiss Axiovert 200 M) at cell passages 1, 3, and 5. Further, immunofluorescence was performed as previously described.⁸ MCF-7 and MCF7-RR cells were incubated with the β -tubulin primary antibody (Cell Signaling, 2128S), followed by 1 h secondary antibody incubation (ThermoFisher, A11029). Imaging was performed using a Zeiss 510 Meta confocal microscope.

Transmission Electron Microscopy. MCF-7 and MCF7-RR cells were fixed at passages 1, 3, and 5 using 3% glutaraldehyde, followed by fixation with 1% osmium tetroxide.

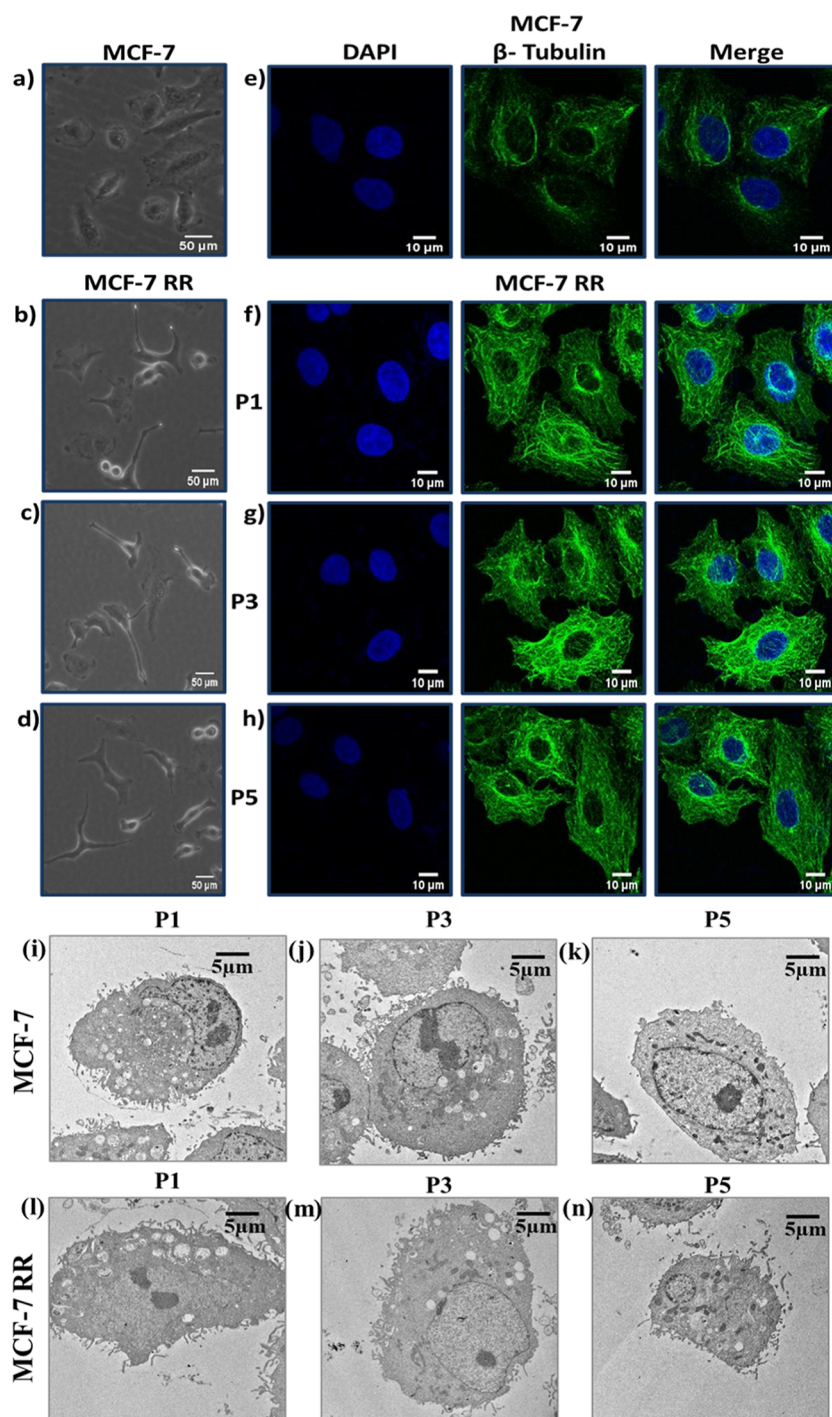


Figure 2. Distinct cytoskeletal and morphological features of radioresistant cells are retained irrespective of the cell passage. Representative phase-contrast microscopy image depicting morphological alterations in (a) MCF7 and (b–d) MCF7-RR cells at passage 1 (P1), passage 3 (P3), and passage 5 (P5), respectively. Scale bar—50 μm . Representative z-stack projection images of immunofluorescence analysis showing changes in the cytoskeletal organization of β -tubulin in (e) MCF7 and (f–h) MCF7-RR cells across different cell passages, P1, P3, and P5. Magnification—40 \times , Scale bar—10 μm . Data were analyzed using ImageJ software. $n = 3$ for all experiments. Representative transmission electron microscopy images depicting ultrastructural changes in (i–k) MCF7 and (l–n) MCF7-RR cells at passage 1 (P1), passage 3 (P3), and passage 5 (P5), respectively. Images were taken at magnification $\times 1500$, and the scale bar depicts 5 μm for electron microscopy images.

Grid contrasting was performed using alcoholic uranyl acetate and lead citrate for 60 and 30 s, respectively. The grids were observed and images were taken under a JEM 1400 Plus transmission electron microscope, JEOL (Japan), at 120 kV, and the analysis was done on iTEM software.

Western Blotting. Total cell lysates were resolved on 12% SDS–polyacrylamide gel electrophoresis, transferred onto a PVDF membrane, and western blot analysis was performed. Antibodies and their dilutions were used as previously described.^{6u}

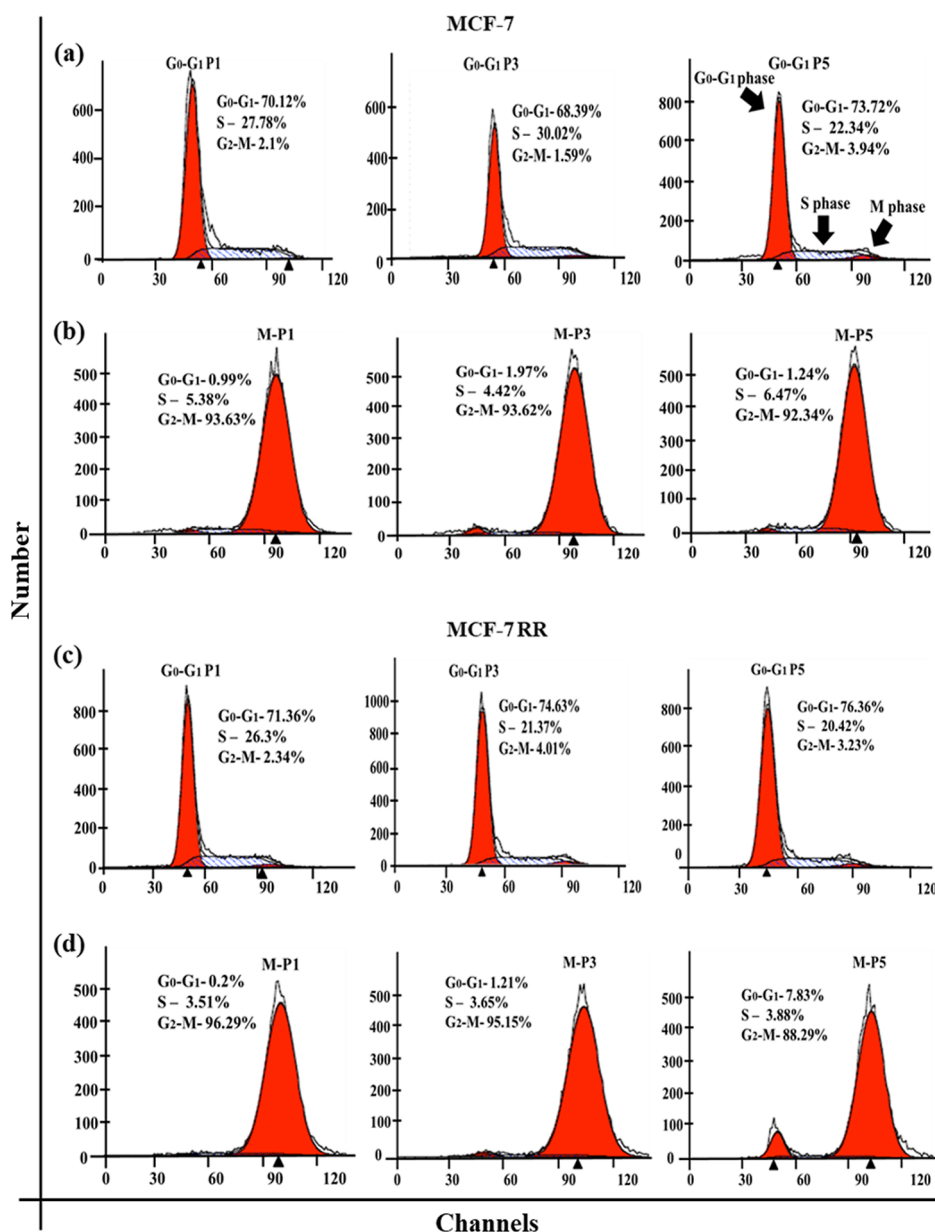


Figure 3. Synchronization of parental and radioresistant cells in the G₀/G₁ and G₂/M phases. Flow cytometry-based cell cycle profile image of parental MCF7 and MCF7-RR synchronized in (a,c) G₀/G₁ and (b,d) G₂/M phases at passage P1, passage P3, and passage P5, respectively. Cells were synchronized in the G₀/G₁ phase by serum starvation, followed by 6 h of serum release in the mitotic phase and incubation with nocodazole for 18 h.

Cell Cycle Analysis. The cell cycle analysis was performed using propidium iodide staining as described earlier.⁸ The acquisition of cells synchronized at the G₀/G₁ phase and the G₂/M phase was carried out using a fluorescence-activated cell sorting (FACS) Calibur flow cytometer (Becton Dickinson), and the analysis was performed using the fluorescence-activated cell sorting (MODFIT) software by Verity house.

Raman Microscopy and Spectral Analysis. Cells (1×10^6) were seeded in a 6-well plate and incubated at 37 °C and 5% CO₂ for 24 h. The parental MCF-7 and MCF7-RR irradiated cell pellets were processed for Raman analysis as described earlier.^{6t} In brief, cell pellets were fixed using 1% paraformaldehyde for 10 mins at 4 °C, centrifuged at 1000 rpm for 3 mins followed by two washes of saline. The cell pellets were placed on a CaF₂ window, and Raman spectra were acquired using a confocal Raman spectroscopy system (WITec alpha 300R, Germany) equipped with a 532 nm diode laser and a 100× objective. Samples were

recorded at 30 mW laser power over 10 accumulations of 10 s. Multiple spectra ($n = 10$) were recorded from different sample areas to examine intra-sample variability. Average spectra ($n = 30$) per group were taken ahead for further analysis.

The spectra were interpolated in the fingerprint region 600–1800 cm⁻¹, smoothed (Savitzky–Golay method and window size 3), and baseline corrected by fitting and subtracting polynomial order 5 using Labspec software. The vector-normalized spectra were subjected to multivariate unsupervised principal component analysis (PCA) and supervised principal component based linear discriminant analysis (PC-LDA). PCA identifies the maximum variance between the data, while PC-LDA provides distinct classification between groups. Unscrambler X software (v.10.4.1, CAMO Software AS) was employed for data analysis.

Statistical Analysis. All experiments were performed in triplicate. The data are presented as the mean \pm S.D. Student's *t*-

test was used for statistical analysis, and the significant differences were considered as per the following criteria: * $P < 0.05$, ** $P < 0.01$, *** $P < 0.001$.

RESULTS

Characterization of Radioresistant MCF7-RR Cell Line.

MCF-7 and MCF7-RR cells at passages 1, 3, and 5 post-revival were exposed to a single fraction of 2, 4, 6, and 8 Gy radiation dose to assess whether the radioresistant properties of MCF7-RR cells were maintained throughout the cell passaging. In concordance with the earlier results, we observed different radiation responses in parental MCF-7 and MCF7-RR cells (Figure 1). The radioresistant MCF7-RR cells showed an increased survival potential compared to the parental MCF-7 cells (Figure 1d–f). The data suggest that no significant difference was observed in the increased survival potential across varying cell passages in the MCF7-RR cells. The radioresistant cells retained the enhanced survival potential with the increasing passage number.

Distinct Cytoskeletal and Morphological Features of Radioresistant Cells are Maintained with Increasing Passage Number.

Morphological features of parental MCF-7 and MCF7-RR cells were studied through phase-contrast, electron, and confocal microscopy to affirm the alteration across different cell passages. Parental MCF-7 cells exhibited a typical epithelial-like morphology, with adhered cells showing cobblestone-like monolayers (Figure 2a). Also, a discernible alteration in cellular morphology was observed with radioresistance development (Figure 2b–d). The radioresistant MCF7-RR cells phenotypically showed an increase in spindle-shaped morphology wherein they contacted each other through focal points rather than the entire cellular area. Interestingly, the morphology of radioresistant cells was maintained with differing cell passages, like cell survival potential. Confocal microscopy-based cytoskeletal analysis revealed that parental MCF-7 cells have typical cytoskeletal organization. In contrast, distorted arrangement and aberrant organization of the cytoskeletal protein β -tubulin in radioresistant MCF7-RR cells across different cell passages (Figure 2e–h) were observed. To further understand the cell-passage-dependent ultrastructural changes, electron microscopic analysis was performed. Parental and radiation-resistant MCF-7 cells displayed enhanced vacuolation, autophagy, and a lower mitochondrial number at cell passage number P1. As the passage number increased to P3, autophagic bodies and vacuolation decreased in MCF-RR compared to that in MCF-7 cells. Moreover, P5 cells attained a well-defined mitochondrial morphology with decreased vacuolation in both parental and resistant cells (Figure 2i–n). Additionally, electron microscopy-based cell size analysis was performed to study passage-dependent cell size alterations. The data showed no significant change in the cell size as the passage number increased from P1 to P5 in MCF-7 and MCF-7 RR cells (Supporting Information, Figure S3). Alteration in mitochondrial dynamics, vacuolation, and activation of autophagy in response to cellular stress has been previously reported.⁹ The observed changes from P1 to P5 suggest a decrease in cellular stress after the revival of cryopreserved cells.

Raman Spectra of Parental and Radioresistant Cell Populations Reveal Unique Cell Cycle-dependent Spectral Features. To understand the alterations occurring across the moderately sensitive G_0/G_1 and the highly radiosensitive G_2/M phases across different cell passages, we carried out a cell cycle-based analysis of parental and radioresistant MCF7 cells.

The parental and radioresistant cells, post-synchronization in the G_0/G_1 and G_2/M phases of the cell cycle, showed no significant difference in the percentage of cells in relation to the passage numbers. The cell percentages in the G_0/G_1 phase with increasing passage (P1, P3, and P5) were 70, 68, 73 and 71, 74, and 76% and in the G_2/M phase, the cell percentages were 93, 93, 92 and 96, 95, and 88%, in parental and radioresistant cells, respectively (Figure 3c,d).

Mean Raman spectra of parental MCF7 and MCF7-RR populations were assessed to identify biochemical alterations at different cell cycle phases (Figure 4). The comparison of parental MCF-7 with MCF7-RR cells synchronized in the G_0/G_1 phase at P1, P3, and P5 showed an overall increased intensity of Raman bands contributing to DNA bases—T, C (788 cm^{-1}), T, A, G (1376 cm^{-1}), A, and G (1491 cm^{-1}), phenylalanine (1009 cm^{-1}), the combined contribution from protein and lipid at C–N stretching, and chain C–C stretch (1125 cm^{-1}), respectively, and resonance Raman bands of cytochrome ($750, 1585\text{ cm}^{-1}$). The low-intensity bands contributed to proteins—amide III β -sheet (1240 cm^{-1}), the combined contribution from protein and lipid at amide III α -helix (1268 cm^{-1}) and CH_2 deformation (1450 cm^{-1}), and amide I (1665 cm^{-1}). In the case of MCF7-RR cells synchronized in the G_2/M phase at P1, P3, and P5, overall increased intensity of Raman bands contributing to nucleic acid features—T, C (788 cm^{-1}), T, A, G (1376 cm^{-1}), protein and lipid overlap region at C–N stretching, and chain C–C stretch (1125 cm^{-1}), respectively, and resonance Raman bands of cytochrome ($750, 1585\text{ cm}^{-1}$) were seen, while decreased intensity bands contributed to a protein and lipid overlap region at amide III α -helix (1268 cm^{-1}), CH_2 deformation (1450 cm^{-1}), and amide I (1665 cm^{-1}). The cell cycle phase-dependent differences in the biochemical components of parental and radioresistant MCF7 cells indicate the distinct alterations occurring in the cells on acquiring radioresistance. The increased intensity of Raman bands contributing to vibrational modes of nucleic acids $788, 1376, \text{ and } 1491\text{ cm}^{-1}$ in MCF7-RR cells indicates increased DNA damage repair post-irradiation and thereby an enhanced radioresistant population (Figure 4). Several proteins involved in DNA repair protect the radiation-treated cells from cell death and increase radioresistance. In contrast, proteins involved in apoptosis induce cell death and enhance radio sensitivity. In addition, similar proteins such as TP53 are involved in cell cycle arrest and apoptosis, compensating for the cell death induced at either of the stages, thereby enhancing radioresistance.¹⁰ The variation in intensities of Raman bands at amide III and amide I across different cell passage numbers and cell cycle phases depicts the alterations in proteins in parental MCF7 and MCF7-RR cells (Figure 4). The spectral variations are distinct from those in cell passage 3, indicating that the modifications in a revived radioresistant cell line are seen as early as passage 3. Around passage 5, the cells demonstrate stabilized features (Figure 4). We further examined the Raman spectral features across different cell passages to ascertain whether these biochemical changes in MCF7-RR cells are persistent. The spectral features are assigned tentatively based on the existing literature.¹¹

Raman Spectral Features Alter in Parental and Radioresistant Cell Populations with Differing Cell Passages. In the context of cell passage, MCF7-RR cells synchronized in the G_0/G_1 phase showed the increased intensity of Raman bands at $750, 1125, 1585, 788, \text{ and } 1376\text{ cm}^{-1}$ until cell passage 5 (Figure 4). The alterations in Raman bands at $1009, 1240, 1268, \text{ and } 1665\text{ cm}^{-1}$ were persistent with the

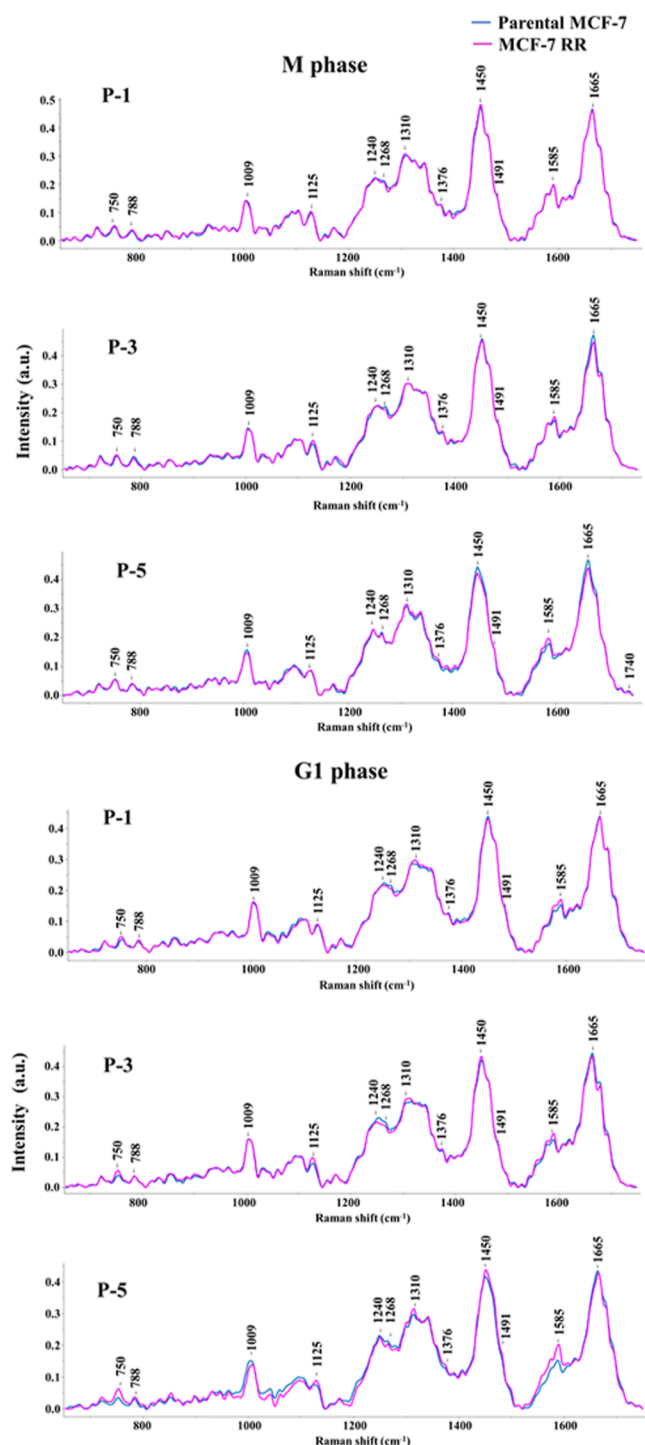


Figure 4. Raman spectra of parental MCF-7 and MCF7-RR cells reveal unique cell cycle-dependent spectral features. The spectra were interpolated in the fingerprint region 600–1800 cm^{-1} . 10 spectra ($n = 10$) were recorded from different areas of the sample for consideration of intra-sample variability. Mean spectra of parental MCF7 and MCF7-RR cells at different cell passages, P1, P3, and P5, synchronized at the G_0/G_1 and G_2/M phases. Experiments were performed in triplicate ($n = 3$).

increasing cell passages. On the other hand, MCF7-RR cells synchronized in the G_2/M phase showed subtle differences in the intensity of Raman bands at 750, 1125, and 1376 cm^{-1} , while distinct alterations were observed at 1009, 1585, 1240, 1268, 1450, and 1665 cm^{-1} , with the increasing cell passage. To further

understand the distinct Raman spectral features, we analyzed the differences between the G_0/G_1 and G_2/M phase synchronized cells at passage 5. Compared to the G_2/M phase, the G_0/G_1 phase MCF7-RR cells at passage 5 showed a higher intensity of resonance Raman bands at 750, 1585, and 1450 cm^{-1} .

To demarcate the spectral differences between the groups, difference Raman spectra were computed by subtracting MCF-7 spectra from MCF-7 RR spectra in the G_0/G_1 and G_2/M phases at Passages 1, 3, and 5. Positive bands were from MCF-7 RR, while negative bands were from MCF-7 cells. In the case of the G_0/G_1 phase at Passage 1, prominent positive bands were observed at 788, 750, and 1585 cm^{-1} , suggesting an overall increase in DNA and cytochromes in these cells. Strong negative peaks were observed at 1268, 1450, and 1665 cm^{-1} , suggesting a reduced protein content in radioresistant cells at an early passage 1 (Figure 5). In passages 3 and 5, strong positive bands were consistently observed at 750 and 1585 cm^{-1} (cytochromes) which might be a distinct spectral feature of radioresistant cells (Figure 5). Negative bands were seen at 1240, 1665, and 1268 cm^{-1} . These changes suggest a decreased protein content in the radioresistant cells compared to that in parental cells.

While during passage 1 in the G_2/M phase, the positive bands were seen at 1125, 750, and 1585 cm^{-1} . Unaltered intensities were observed at 788, 1240, 1268, and 1376 cm^{-1} , while a negative band was observed at 1009 cm^{-1} (phenylalanine), contributing toward an overall varied biochemical profile at an early passage 1. At P3, positive bands were seen at 750, 1125, and 1585 cm^{-1} , while negative bands were seen at 1665, 1268, and 788 cm^{-1} , and in passage 5, strong positive bands appeared at 1585 cm^{-1} and negative bands were observed at 1009, 1450, and 1665 cm^{-1} (Figure 5). We observed an overall increase in cytochrome features (750 and 1585 cm^{-1}) at the G_0/G_1 and G_2/M phases with an increase in passage number which hints at it being a radioresistance-induced biochemical feature (Supporting Information, Figure S4). Moreover, metabolic reprogramming is a key feature of radioresistant cells to meet the energy requirements compared to the tumor cells.¹² Therefore, the increase in cytochromes is in coherence with the observed mitochondrial alteration with the increasing passage number. A decrease in 1665 cm^{-1} (amide I) with the increasing passage number indicates at it being a stabilizing biochemical stratification. The altered balance of protein and DNA spectral features means varied cellular mechanisms at different cell cycle passages in parental and resistant cells. To ascertain the effect of cell cycle and passage-dependent biochemical alterations, we assessed the levels of some key cell growth molecules in MCF-7 and MCF-7 RR cells at P1, P3, and P5.

Level of MAP Kinases in Parental and Resistant Cells at Various Passages.

Activation of the MAPK (mitogen-activated protein kinase) pathway in response to cell growth and stress responses is well-known.¹³ The levels of MAPK pathway effector molecules with cell passages 1, 3, and 5 in the G_1 and M phases of MCF-7 and MCF-7 RR cells were studied. The pp38 levels were significantly higher at passage 1 after revival, followed by a decreasing pattern till passage 5 in MCF-7 cells; however, the inverse pattern of pp38 levels was observed in MCF-7 RR cells. On the other hand, pERK levels were increased with the passage number in parental cells, whereas in the resistant cells, pERK levels plateaued at passages 3 and 5 in the G_1 phase of the cell cycle (Figure 6a). During the M phase, the level of pp38 and pERK protein increased with the passage number in MCF-7 as well as MCF-7 RR cells (Figure 6b). Parental and radioresistant cells respond differently under

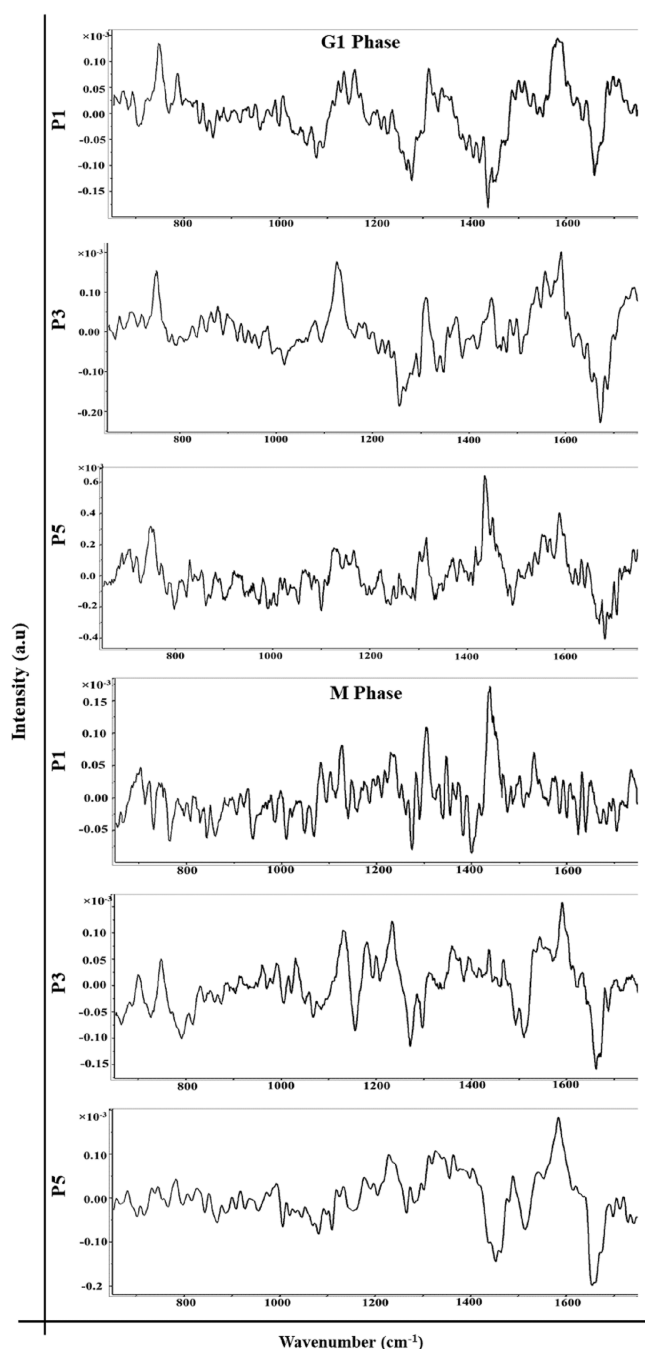


Figure 5. Difference spectra of parental MCF-7 and MCF7-RR cells delineate cell passage-dependent spectral features. Difference Raman spectra were computed by subtracting MCF7 spectra from MCF7-RR spectra in the G_0/G_1 and G_2/M phases at Passages 1, 3, and 5. Positive peaks represent MCF7-RR cells and negative peaks represent MCF7 parental cells.

varying cell passage numbers and cell cycle phases, corroborating our earlier observation of altered Raman protein features (Figure 5). The alteration in the levels of MAPK proteins suggests that cells experience cellular stress after immediate revival. Therefore, the optimum passage number of a cell line with stabilized protein expression should be used for further studies.

Multivariate Data Analyses Identify Cell Cycle and Cell Passage-Dependent Distinct Clusters of Parental and Radioresistant Cells. The parental and radioresistant cells

were classified using the multivariate data analysis tools, PCA, and PC-LDA. The unsupervised PCA was performed for both parental MCF-7 and MCF7-RR synchronized at different cell cycle phases— G_0/G_1 and G_2/M , which showed unique clusters of parental MCF-7 and MCF7-RR at different cell cycle phases (Figure 7a–f). Cells in the G_0/G_1 phase showed unique clusters throughout the cell passaging. However, overlapping clusters were seen in cell passage 1 of the G_2/M phase (Figure 7d), while distinguished clusters were seen from passage 3 onward (Figure 7e,f). Further, supervised PC-LDA was performed to stratify parental MCF-7 and MCF7-RR cells.

PC-LDA, using scores of the first two PCs, of the G_0/G_1 and G_2/M phase synchronized parental MCF-7 and MCF7-RR cells showed non-overlapping clusters with increasing cell passage. The G_0/G_1 and G_2/M phase parental and MCF7-RR cells were classified with 71.67, 80, 81.67, and 49.15, 71.67, and 70%, respectively. As shown in the data, the classification efficiency in PC-LDA increased in the G_0/G_1 phase from 71.67% in passage 1 to 81.67% in passage 5, while that in the G_2/M phase increased from 49.15% in passage 1 to 70% in passage 5. The PCA loadings of the respective groups are provided in the Supporting Information, Figure S1.

The unique clusters seen in the G_0/G_1 phase at different cell passages imply that the biochemical profile of the radioresistant cells in the G_0/G_1 phase is altered from cell passage 1 (Figure 7a–c). A previous study by Matthews et al. on irradiated DU145 cells showed cell arrest in the G_2/M phase and decreased DNA content in the G_0/G_1 phase.⁶ⁿ Additionally, the G_0/G_1 peak observed at 120 h implied that a fraction of G_2/M arrested cells successfully repaired radiation-induced DNA damage to complete a mitotic division. Similarly, our findings of distinct clusters of the MCF7-RR G_0/G_1 phase across different cell passages validate that the radioresistant cells had undergone DNA damage repair and subsequent mitotic divisions and acquired distinct radioresistance characteristics as compared to parental MCF-7. On the other hand, the decrease in overlapping clusters in the G_2/M phase with the increasing passage implies that biochemical alterations are achieved at a latter cell passage, where the features of radioresistant cells are distinct from the parental cells (Figure 7d–f). Similar findings were seen in the spectral characteristics of the G_0/G_1 and G_2/M phases at the higher cell passage, 5 (Figure 4). Moreover, the increasing nucleic acid features and alterations in protein features indicate the proliferating population of the radioresistant cells—MCF7-RR, with increasing cell passages. The confusion matrix identified true classifiers as diagonal elements and misclassifiers as ex-diagonal elements. The variations in the group are represented by true classifiers, while misclassifications denote the similarities between them. The confusion matrix correctly classified 77 to 87% of the G_0/G_1 phase parental MCF-7 cells and 67 to 83% of the MCF7-RR cells across different cell passages (Figure 8a–c). Similarly, 60 to 66% of parental MCF-7 cells in the G_2/M phase and 40 to 83% of the MCF7-RR cells were correctly classified with differing cell passages (Figure 8d–f and Supporting Information, Figure S2). Misclassification of parental MCF-7 and MCF7-RR cells decreased with the increasing cell passage. Cells in the G_0/G_1 phase showed 23 to 13 and 33 to 17% misclassification, while the G_2/M phase cells showed 40 to 43 and 60 to 16% misclassification of parental MCF-7 and MCF7-RR cells across different cell passages, respectively. PC-LDA showed a lower classification—49.15%, at the earlier passage in the G_2/M phase. In contrast, the higher and similar classifications at cell passage 3 (71.67%) and cell passage

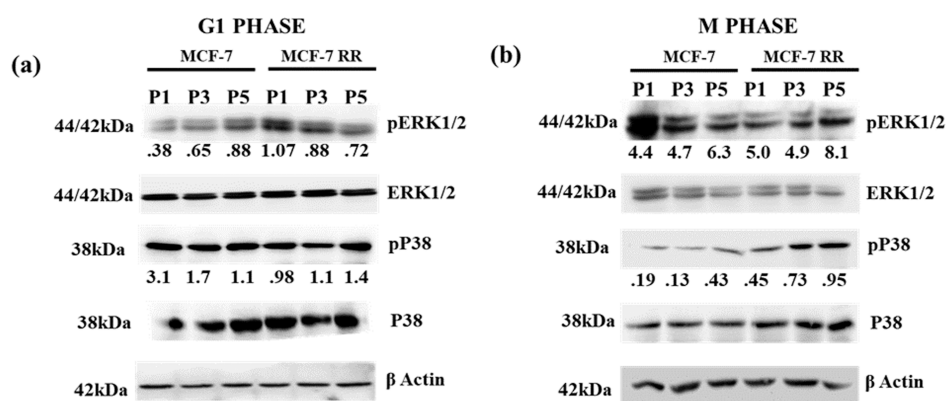


Figure 6. Western blot of MAP kinases in MCF-7 and MCF7-RR cells at passage 1 (P1), passage 3 (P3), and passage 5 (P5). (a) pp38 and pERK levels at P1, P3, and P5 in the G_0/G_1 phase. (b) pP38 and pERK levels at P1, P3, and P5 in the G_2/M phase. Protein quantification was done using ImageJ software. β -actin was used as a loading control. Phospho-protein levels were estimated from total protein levels.

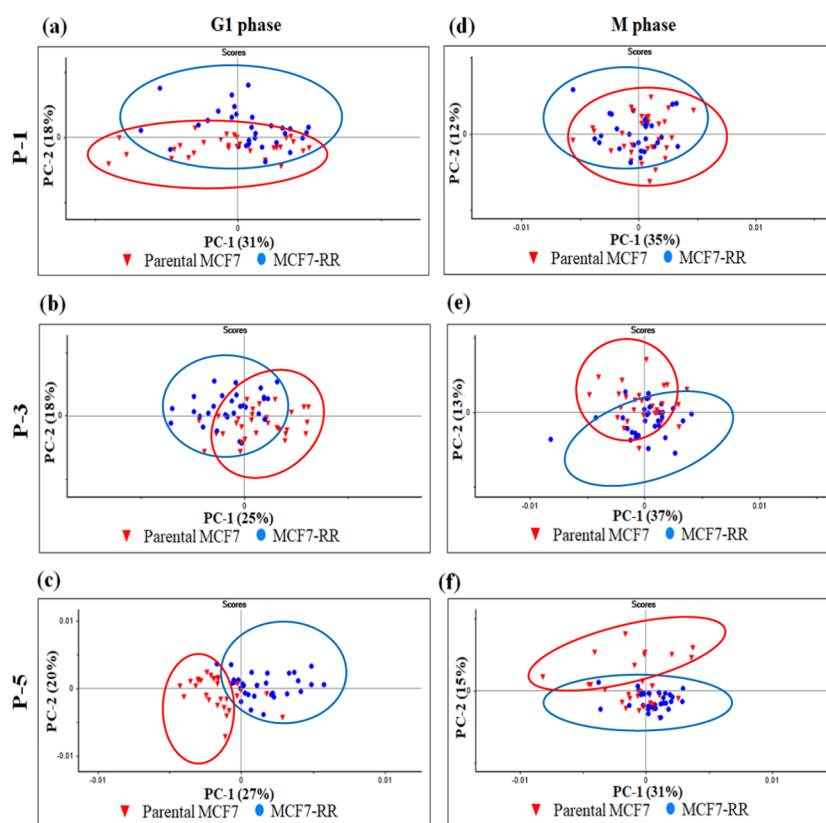


Figure 7. PCA classifies parental MCF-7 and MCF7-RR cells across different cell passages. Scatter plot for unsupervised PCA of parental MCF7 and MCF7-RR cells synchronized at (a–c) G_0/G_1 and (d–f) G_2/M phases across varying cell passages. PCA identifies the maximum variance between the data.

5 (70%) (Figure 8d–f) are indicative of stabilized characteristics of radioresistant cells at a higher passage.

DISCUSSION AND CONCLUSIONS

Radiation treatment induces DNA damage through direct and indirect mechanisms, eventually causing cell death. Although fractionated radiotherapy is effective in cell killing, some tumor cells evade cell death due to defects in cell cycle checkpoints, leading to resistance where the radioresistant cells have a better survival advantage over the parental cells.^{2d,10,14} The *in vitro* generated radioresistance cells are often cryopreserved, and cells are revived as and when required for experiments. The

present study highlights the biochemical alterations at varying cell passages based on Raman spectroscopy. The data of MAP kinases showed that the parental and RR cells are susceptible to changes in the level of active phosphoproteins during the passing from P1 to P5 after revival in both the phases of the cells. However, there is no significant difference in the percentage of synchronized cells in either the G_0/G_1 or G_2/M phase between parental and resistant MCF-7 cells (Figure 3). A recent study by Abramczyk et al. showed a correlation between the intensity of cytochrome Raman bands (750 and 1585 cm^{-1}) and the different grades of breast and brain cancer tissue and cell lines.¹⁵ Our earlier studies have shown increased intensity of cytochrome bands in short-term radiation-exposed MCF-7 and

(a)	G_0/G_1 phase			(d)	G_2/M phase		
	MCF-7	MCF-7 RR			MCF-7	MCF-7 RR	
P1	MCF-7	23	10	P1	MCF-7	18	18
	MCF-7 RR	7	20		MCF-7 RR	12	12
(b)	G_0/G_1 phase			(e)	G_2/M phase		
	MCF-7	MCF-7 RR			MCF-7	MCF-7 RR	
P3	MCF-7	23	5	P3	MCF-7	20	7
	MCF-7 RR	7	25		MCF-7 RR	10	23
(c)	G_0/G_1 phase			(f)	G_2/M phase		
	MCF-7	MCF-7 RR			MCF-7	MCF-7 RR	
P5	MCF-7	26	7	P5	MCF-7	17	5
	MCF-7 RR	4	23		MCF-7 RR	13	25

Figure 8. PC-LDA confusion matrix of parental MCF-7 and MCF7-RR cells. Confusion matrix-based classification of parental MCF7 and MCF7-RR cells synchronized at (a–c) G_0/G_1 and (d–f) G_2/M phases across varying cell passages. PC-LDA increases classification efficiency and provides distinct classification between groups.

gingivobuccal carcinoma-derived ITOC-03 cells.^{6t,16} Corroborating our earlier findings, here we report a similar increase in cytochrome Raman bands at 1585 and 750 cm^{-1} in radioresistant MCF-7 cells compared to that in parental MCF-7 cells. Studies have shown that radiation-induced ROS levels cause DNA damage, mitochondrial outer membrane permeabilization, the release of mitochondrial cytochrome C into the cytoplasm, activation of caspases, and eventually apoptosis.¹⁷ However, the observed increased level of cytochromes in radioresistant cells is not associated with cell death and morphological alterations compared to parental MCF-7. Therefore, our findings of induced cytochromes in radiation-treated and radioresistant MCF-7 cell lines might suggest modifications of the cytochromes' redox state, which could be indicative of a "radiation-induced marker".^{6t,16b} However, further biological assays are warranted to ascertain the role of cytochromes in radiation-treated and radioresistant cells. Also, the spectral features, PCA, and PC-LDA findings highlight the differential effect of radiotherapy on the radiosensitive G_2/M phase compared to that on the G_0/G_1 phase and imply that the acquired radioresistance characteristics stabilize in the G_2/M phase synchronized cells at latter passages on cell revival.

Our findings demonstrate enhanced survival potential and stabilization of ultrastructural alterations with distinct spectral features during an increase in the cell passage number in parental and radioresistant MCF-7 cells. To the best of our knowledge, this is the first report suggesting that cell passaging helps decrease cellular stress and is an essential determinant for performing in vitro experiments to get consistent results. Moreover, identifying cytochrome as a "radiation-induced marker" paves the way for exploring the possible role of radiotherapy-induced cytochromes in patients.

■ ASSOCIATED CONTENT

SI Supporting Information

The Supporting Information is available free of charge at <https://pubs.acs.org/doi/10.1021/acsomega.2c06787>.

PCA loadings of parental MCF-7 and MCF7-RR cells of G_0/G_1 and G_2/M phases at passages P1, P3, and P5; confusion matrix-based classification of MCF-7 and MCF7-RR cells plotted as percent versus cell cycle phases. P1: cell passage 1, P3: cell passage 3, P5: cell passage 5; transmission electron microscopy-based cell size measurement in asynchronous MCF-7 and MCF-7 RR cell lines at P1: cell passage 1, P3: cell passage 3, P5: cell passage 5; and overlay plot for difference spectra of parental MCF7 and MCF7-RR cells in G_0/G_1 and G_2/M phases at passages 1, 3, and 5 (PDF)

■ AUTHOR INFORMATION

Corresponding Authors

Murali Krishna Chilakapati – Advanced Centre for Treatment, Research, and Education in Cancer, Tata Memorial Centre, Cancer Research Institute, Navi Mumbai, Maharashtra 410210, India; Training School Complex, Homi Bhabha National Institute, Mumbai, Maharashtra 400085, India; orcid.org/0000-0002-4974-8533; Email: mchilakapati@actrec.gov.in

Sanjay Gupta – Advanced Centre for Treatment, Research, and Education in Cancer, Tata Memorial Centre, Cancer Research Institute, Navi Mumbai, Maharashtra 410210, India; Training School Complex, Homi Bhabha National Institute, Mumbai, Maharashtra 400085, India; Email: sgupta@actrec.gov.in

Authors

Sukanya Rauniyar – Advanced Centre for Treatment, Research, and Education in Cancer, Tata Memorial Centre, Cancer Research Institute, Navi Mumbai, Maharashtra 410210, India; Training School Complex, Homi Bhabha National Institute, Mumbai, Maharashtra 400085, India

Kshama Pansare – Advanced Centre for Treatment, Research, and Education in Cancer, Tata Memorial Centre, Cancer Research Institute, Navi Mumbai, Maharashtra 410210, India

Asmita Sharda – Advanced Centre for Treatment, Research, and Education in Cancer, Tata Memorial Centre, Cancer Research Institute, Navi Mumbai, Maharashtra 410210, India; Training School Complex, Homi Bhabha National Institute, Mumbai, Maharashtra 400085, India; Present

Address: Chromosome Integrity Group, M.R.C. Oxford Institute for Radiation Oncology, Department of Oncology, University of Oxford, Old Road Campus Research Building, Oxford, OX3 7DQ, United Kingdom

Saurav Raj Singh – Advanced Centre for Treatment, Research, and Education in Cancer, Tata Memorial Centre, Cancer Research Institute, Navi Mumbai, Maharashtra 410210, India

Panchali Saha – Advanced Centre for Treatment, Research, and Education in Cancer, Tata Memorial Centre, Cancer Research Institute, Navi Mumbai, Maharashtra 410210, India; Training School Complex, Homi Bhabha National Institute, Mumbai, Maharashtra 400085, India

Complete contact information is available at:

<https://pubs.acs.org/doi/10.1021/acsomega.2c06787>

Author Contributions

This study was carried out under the supervision of S.G. and M.K.C. S.G. conceived the idea. S.R., K.P., A.S., S.G., and M.K.C. contributed to the experimental design. S.R., K.P., A.S., and S.R.S. performed the experiments, and S.R., K.P., and P.S.

analyzed the data. S.R. and K.P. prepared the article. S.R., K.P., S.G., and M.K.C. reviewed the data and finalized the article. S.R. and K.P. contributed equally.

Notes

The authors declare no competing financial interest.

ACKNOWLEDGMENTS

The authors want to sincerely thank the flow cytometry facility and the Department of radiation oncology in ACTREC for their assistance in carrying out the experiments. Special thanks to the SERB, Department of Science and Technology (DST)—India and Advanced Centre for Treatment Research and Education in Cancer (ACTREC), for funds. The Raman microscope employed in the study was procured from DBT Indo-Finnish Project (BT/IN/Indo-Finnish/04/MKC/2014).

REFERENCES

- (1) (a) Baskar, R.; Dai, J.; Wenlong, N.; Yeo, R.; Yeoh, K.-W. Biological response of cancer cells to radiation treatment. *Front. Mol. Biosci.* **2014**, *1*, 24. (b) Debeb, B. G.; Xu, W.; Woodward, W. A. Radiation resistance of breast cancer stem cells: understanding the clinical framework. *J. Mammary Gland Biol. Neoplasia* **2009**, *14*, 11.
- (2) (a) Speers, C.; Zhao, S.; Liu, M.; Bartelink, H.; Pierce, L. J.; Feng, F. Y. Development and Validation of a Novel Radiosensitivity Signature in Human Breast Cancer. *Clin. Cancer Res.* **2015**, *21*, 3667–3677. (b) Villalobos, M. Radiosensitivity of human breast cancer cell lines of different hormonal responsiveness. Modulatory effects of oestradiol. *Int. J. Radiat. Biol.* **1996**, *70*, 161. (c) Holliday, D. L.; Speirs, V. Choosing the right cell line for breast cancer research. *Breast Cancer Res.* **2011**, *13*, 251. (d) Gray, M.; Turnbull, A. K.; Ward, C.; Meehan, J.; Martínez-Pérez, C.; Bonello, M.; Pang, L. Y.; Langdon, S. P.; Kunkler, I. H.; Murray, A.; Argyle, D. Development and characterisation of acquired radioresistant breast cancer cell lines. *Radiat. Oncol.* **2019**, *14*, 64.
- (3) (a) Yadav, P.; Shankar, B. S. Radio resistance in breast cancer cells is mediated through TGF- β signalling, hybrid epithelial-mesenchymal phenotype and cancer stem cells. *Biomed. Pharmacother.* **2019**, *111*, 119–130. (b) Arnold, C. R.; Mangesius, J.; Skvortsova, I.-I.; Ganswindt, U. The Role of Cancer Stem Cells in Radiation Resistance. *Front. Oncol.* **2020**, *10*, 164. (c) Choi, J.; Yoon, Y. N.; Kim, N.; Park, C. S.; Seol, H.; Park, I.-C.; Kim, H.-A.; Noh, W. C.; Kim, J.-S.; Seong, M.-K. Predicting Radiation Resistance in Breast Cancer with Expression Status of Phosphorylated S6K1. *Sci. Rep.* **2020**, *10*, 641. (d) Perez-Añorbe, I. X.; Gonzalez-De la Rosa, C. H.; Soto-Reyes, E.; Beltran-Anaya, F. O.; Del Moral-Hernandez, O.; Salgado-Albarran, M.; Angeles-Zaragoza, O.; Gonzalez-Barrios, J. A.; Landero-Huerta, D. A.; Chavez-Saldaña, M.; Garcia-Carranca, A.; Villegas-Sepulveda, N.; Arechaga-Ocampo, E. New insights into radioresistance in breast cancer identify a dual function of miR-122 as a tumor suppressor and oncomiR. *Mol. Oncol.* **2019**, *13*, 1249–1267. (e) Pearce, A. G.; Segura, T. M.; Rintala, A. C.; Rintala-Maki, N. D.; Lee, H. The generation and characterization of a radiation-resistant model system to study radioresistance in human breast cancer cells. *Radiat. Res.* **2001**, *156*, 739–750.
- (4) (a) Baust, J. G.; Gao, D.; Baust, J. M. Cryopreservation: An emerging paradigm change. *Organogenesis* **2009**, *5*, 90–96. (b) Kumar, A.; Prasad, J. K.; Srivastava, N.; Ghosh, S. K. Strategies to Minimize Various Stress-Related Freeze–Thaw Damages During Conventional Cryopreservation of Mammalian Spermatozoa. *Biopreserv. Biobanking* **2019**, *17*, 603–612.
- (5) (a) Ahmed, K. M.; Li, J. J. NF-kappa B-mediated adaptive resistance to ionizing radiation. *Free Radical Biol. Med.* **2008**, *44*, 1–13. (b) Chang, L.; Graham, P. H.; Hao, J.; Ni, J.; Bucci, J.; Cozzi, P. J.; Kearsley, J. H.; Li, Y. PI3K/Akt/mTOR pathway inhibitors enhance radiosensitivity in radioresistant prostate cancer cells through inducing apoptosis, reducing autophagy, suppressing NHEJ and HR repair pathways. *Cell Death Dis.* **2014**, *5*, No. e1437. (c) Huang, R.-X.; Zhou, P.-K. DNA damage response signaling pathways and targets for radiotherapy sensitization in cancer. *Signal Transduction Targeted Ther.* **2020**, *5*, 254. (d) Haverty, P. M.; Lin, E.; Tan, J.; Yu, Y.; Lam, B.; Lianoglou, S.; Neve, R. M.; Martin, S.; Settleman, J.; Yauch, R. L.; Bourgon, R. Reproducible pharmacogenomic profiling of cancer cell line panels. *Nature* **2016**, *533*, 333–337.
- (6) (a) Redd, D. C. B.; Feng, Z. C.; Yue, K. T.; Gansler, T. S. Raman Spectroscopic Characterization of Human Breast Tissues: Implications for Breast Cancer Diagnosis. *Appl. Spectrosc.* **2016**, *47*, 787–791. (b) Singh, S. P.; Deshmukh, A.; Chaturvedi, P.; Murali Krishna, C. In vivo Raman spectroscopic identification of premalignant lesions in oral buccal mucosa. *J. Biomed. Opt.* **2012**, *17*, 1050021. (c) Sahu, A.; Sawant, S.; Mangain, H.; Krishna, C. M. Raman spectroscopy of serum: an exploratory study for detection of oral cancers. *Analyst* **2013**, *138*, 4161. (d) Haka, A. S.; Volynskaya, Z.; Gardecki, J. A.; Nazemi, J.; Lyons, J.; Hicks, D.; Fitzmaurice, M.; Dasari, R. R.; Crowe, J. P.; Feld, M. S. In vivo Margin Assessment during Partial Mastectomy Breast Surgery Using Raman Spectroscopy. *Cancer Res.* **2006**, *66*, 3317–3322. (e) Shipp, D. W.; Rakha, E. A.; Koloydenko, A. A.; Macmillan, R. D.; Ellis, I. O.; Notingher, I. Intra-operative spectroscopic assessment of surgical margins during breast conserving surgery. *Breast Cancer Res.* **2018**, *20*, 69. (f) Sahu, A.; Nandakumar, N.; Sawant, S.; Krishna, C. M. Recurrence prediction in oral cancers: a serum Raman spectroscopy study. *Analyst* **2015**, *140*, 2294–2301. (g) Malik, A.; Sahu, A.; Singh, S. P.; Deshmukh, A.; Chaturvedi, P.; Nair, D.; Nair, S.; Murali Krishna, C. In vivo Raman spectroscopy-assisted early identification of potential second primary/recurrences in oral cancers: An exploratory study. *Head Neck* **2017**, *39*, 2216–2223. (h) Krishna, C. M.; Sockalingum, G. D.; Vadhiraja, B. M.; Maheedhar, K.; Rao, A. C. K.; Rao, L.; Venteo, L.; Pluot, M.; Fernandes, D. J.; Vidyasagar, M. S.; Kartha, V. B.; Manfait, M. Vibrational spectroscopy studies of formalin-fixed cervix tissues. *Biopolymers* **2007**, *85*, 214–221. (i) Vidyasagar, M. S.; Maheedhar, K.; Vadhiraja, B. M.; Fernandes, D. J.; Kartha, V. B.; Muralikrishna, C. Raman Spectroscopy of Tissues Collected at Different Fractions of Radiation Therapy: Response Assessment to Radiotherapy in Cervix Cancers. *Int. J. Radiat. Oncol., Biol., Phys.* **2007**, *69*, S388–S389. (j) Pansare, K.; Pillai, D.; Parab, S.; Singh, S. R.; Kannan, S.; Ludbe, M.; Hole, A.; Murali Krishna, C.; Gera, P. Quality assessment of cryopreserved biospecimens reveals presence of intact biomolecules. *J. Biophotonics* **2019**, *12*, No. e201960048. (k) Vidyasagar, M. S.; Maheedhar, K.; Vadhiraja, B. M.; Fernandes, D. J.; Kartha, V. B.; Krishna, C. M. Prediction of radiotherapy response in cervix cancer by Raman spectroscopy: A pilot study. *Biopolymers* **2008**, *89*, 530–537. (l) Rubina, S.; Vidyasagar, M. S.; Murali Krishna, C. Raman Spectroscopic Study on Prediction of Treatment Response in Cervical Cancers. *J. Innovative Opt. Health Sci.* **2013**, *06*, 1350014. (m) Paidi, S. K.; Diaz, P. M.; Dadgar, S.; Jenkins, S. V.; Quick, C. M.; Griffin, R. J.; Dings, R. P. M.; Rajaram, N.; Barman, I. Label-Free Raman Spectroscopy Reveals Signatures of Radiation Resistance in the Tumor Microenvironment. *Cancer Res.* **2019**, *79*, 2054–2064. (n) Matthews, Q.; Brolo, A. G.; Lum, J.; Duan, X.; Jirasek, A. Raman spectroscopy of single human tumour cells exposed to ionizing radiation in vitro. *Phys. Med. Biol.* **2011**, *56*, 19–38. (o) Matthews, Q.; Jirasek, A.; Lum, J. J.; Brolo, A. G. Biochemical signatures of in vitro radiation response in human lung, breast and prostate tumour cells observed with Raman spectroscopy. *Phys. Med. Biol.* **2011**, *56*, 6839–6855. (p) Yasser, M.; Shaikh, R.; Chilakapati, M. R.; Teni, T. Raman Spectroscopic Study of Radioresistant Oral Cancer Sublines Established by Fractionated Ionizing Radiation. *PLoS One* **2014**, *9*, No. e97777. (q) Harder, S. J.; Matthews, Q.; Isabelle, M.; Brolo, A. G.; Lum, J. J.; Jirasek, A. A Raman Spectroscopic Study of Cell Response to Clinical Doses of Ionizing Radiation. *Appl. Spectrosc.* **2015**, *69*, 193–204. (r) Kaur, E.; Sahu, A.; Hole, A. R.; Rajendra, J.; Chaubal, R.; Gardi, N.; Dutt, A.; Moiyadi, A.; Krishna, C. M.; Dutt, S. Unique spectral markers discern recurrent Glioblastoma cells from heterogeneous parent population. *Sci. Rep.* **2016**, *6*, 26538. (s) Harder, S. J.; Isabelle, M.; DeVorkin, L.; Smazynski, J.; Beckham, W.; Brolo, A. G.; Lum, J. J.; Jirasek, A. Raman spectroscopy identifies radiation response in human non-small cell lung cancer xenografts. *Sci. Rep.* **2016**, *6*, 21006. (t) Pansare, K.; Raj Singh, S.; Chakravarthy, V.; Gupta, N.; Hole,

A.; Gera, P.; Sarin, R.; Murali Krishna, C. Raman Spectroscopy: An Exploratory Study to Identify Post-Radiation Cell Survival. *Appl. Spectrosc.* **2020**, *74*, 553–562. (u) Sharda, A.; Rashid, M.; Shah, S. G.; Sharma, A. K.; Singh, S. R.; Gera, P.; Chilkapati, M. K.; Gupta, S. Elevated HDAC activity and altered histone phospho-acetylation confer acquired radio-resistant phenotype to breast cancer cells. *Clin. Epigenet.* **2020**, *12*, 4.

(7) Franken, N. A. P.; Rodermond, H. M.; Stap, J.; Haveman, J.; van Bree, C. Clonogenic assay of cells in vitro. *Nat. Protoc.* **2006**, *1*, 2315–2319.

(8) Sharma, A. K.; Bhattacharya, S.; Khan, S. A.; Khade, B.; Gupta, S. Dynamic alteration in H3 serine 10 phosphorylation is G1-phase specific during ionization radiation induced DNA damage response in human cells. *Mutat. Res., Fundam. Mol. Mech. Mutagen.* **2015**, *773*, 83–91.

(9) (a) Picard, M.; McEwen, B. S.; Epel, E. S.; Sandi, C. An energetic view of stress: Focus on mitochondria. *Front. Neuroendocrinol.* **2018**, *49*, 72–85. (b) Kroemer, G.; Mariño, G.; Levine, B. Autophagy and the integrated stress response. *Mol. Cell* **2010**, *40*, 280–293. (c) Shubin, A. V.; Demidyuk, I. V.; Komissarov, A. A.; Rafieva, L. M.; Kostrov, S. V. Cytoplasmic vacuolization in cell death and survival. *Oncotarget* **2016**, *7*, 55863–55889.

(10) Jorgensen, T. J. Enhancing radiosensitivity: Targeting the DNA repair pathways. *Cancer Biol. Ther.* **2014**, *8*, 665–670.

(11) (a) Parker, F. S. *Applications of Infrared, Raman, and Resonance Raman Spectroscopy in Biochemistry*; Springer: New York, NY, 1983. (b) Talari, A. C. S.; Movasaghi, Z.; Rehman, S.; Rehman, I. u. Raman Spectroscopy of Biological Tissues. *Appl. Spectrosc. Rev.* **2014**, *50*, 46–111.

(12) Lynam-Lennon, R.; Maher, N.; Maguire, S. G.; Phelan, A.; Muldoon, J.; Reynolds, C.; O'Sullivan, J. V.; O'Sullivan, J. Altered Mitochondrial Function and Energy Metabolism Is Associated with a Radioresistant Phenotype in Oesophageal Adenocarcinoma. *PLoS One* **2014**, *9*, No. e100738.

(13) Rezatabar, S.; Karimian, A.; Rameshknia, V.; Parsian, H.; Majidinia, M.; Kopi, T. A.; Bishayee, A.; Sadeghinia, A.; Yousefi, M.; Monirialamdari, M.; Yousefi, B. RAS/MAPK signaling functions in oxidative stress, DNA damage response and cancer progression. *J. Cell. Physiol.* **2019**, *234*, 14951.

(14) Qi, X. S.; Pajonk, F.; McCloskey, S.; Low, D. A.; Kupelian, P.; Steinberg, M.; Sheng, K. Radioresistance of the breast tumor is highly correlated to its level of cancer stem cell and its clinical implication for breast irradiation. *Radiother. Oncol.* **2017**, *124*, 455–461.

(15) Abramczyk, H.; Surmacki, J. M.; Brozek-Pluska, B.; Kopec, M. Revision of Commonly Accepted Warburg Mechanism of Cancer Development: Redox-Sensitive Mitochondrial Cytochromes in Breast and Brain Cancers by Raman Imaging. *Cancers* **2021**, *13*, 2599.

(16) (a) Pansare, K.; Gardi, N.; Kamat, S.; Dange, P.; Previn, R.; Gera, P.; Kowtal, P.; Amin, K.; Sarin, R. Establishment and genomic characterization of gingivobuccal carcinoma cell lines with smokeless tobacco associated genetic alterations and oncogenic PIK3CA mutation. *Sci. Rep.* **2019**, *9*, 8272. (b) Pansare, K.; Vaid, A.; Singh, S. R.; Rane, R.; Visani, A.; Ranjan, M.; Krishna, C. M.; Sarin, R.; Joseph, A. Effect of Cold Atmospheric Plasma Jet and Gamma Radiation Treatments on Gingivobuccal Squamous Cell Carcinoma and Breast Adenocarcinoma Cells. *Plasma Chem. Plasma Process.* **2021**, *42*, 163–178.

(17) Cairns, R. A.; Harris, I. S.; Mak, T. W. Regulation of cancer cell metabolism. *Nat. Rev. Cancer* **2011**, *11*, 85–95.